Turkish Journal of Electrical Engineering & Computer Sciences

http://journals.tubitak.gov.tr/elektrik/

Research Article

Turk J Elec Eng & Comp Sci
(2019) 27: 3219 – 3233

doi:10.3906/elk-1805-149

Fault-tolerant control of a PMSG-based wind turbine based on parallel interleaved converters

Mohamed ABBES[1,2]

[1]National School of Engineering of Tunis (ENSIT), University of Tunis, Tunis, Tunisia
[2]Laboratory of Technologies of Information, Communication, and Electrical Engineering (LaTICE) Tunis, Tunisia

Received: 22.05.2018 • **Accepted/Published Online:** 08.04.2019 • **Final Version:** 26.07.2019

Abstract: Lowering the cost of wind energy has been one of the main objectives of the wind industry in the past years. To achieve this objective, considerable research efforts have been made to improve the availability of wind turbines. Recent statistical analyses have shown that frequency converters are among the most frequently failing components for variable speed wind systems. Therefore, several configurations were proposed in the literature to improve the availability of these generating devices. These configurations are mainly based on the redundancy of power converters (active and standby) or the converter bypass technique. However, for the special case of PMSG-based wind turbines, the power electronic subsystem cannot be bypassed and redundancy will significantly increase the cost of the overall structure since fully rated converters are used. Therefore, this paper proposes a new design for PMSG-based wind turbines based on parallel interleaved converters and a fault-tolerant control strategy. In the proposed configuration, the generator-side and the grid-side converters are made with two parallel interleaved converters with separate DC links. The design is intended to offer continuity of service in the event of converter failure with low additional costs. The design, simulation, and advantages of the proposed configuration are detailed throughout the paper.

Key words: Wind turbines, permanent magnet synchronous generator, parallel interleaved converter, fault-tolerant control

1. Introduction

According to recent studies, reliability and availability are among the crucial factors to increase the competitiveness of wind energy [1]. Several initiatives have been undertaken to identify the weak points in wind generation systems. For example, in the ReliaWind project, field-failure data of more than 350 onshore variable speed wind turbines were analyzed [2]. The dataset covers the period between 2008 and 2011. The results show that the failure rate of power converters reaches 13% just behind the pitch system, which equals 21%. Power converter failures lead to turbine downtimes, increased maintenance costs, and reduced overall availability of the wind system [3]. Consequently, advanced fault-tolerant techniques along with innovative configurations of power converters were introduced in order to improve the performances of these elements [4]. For the doubly-fed induction generator technology, a converter bypass was proposed in [5]. With this solution, the wind turbine operates temporarily in the fixed-speed mode instead of the default variable-speed mode. Active- or standby-redundant converters were investigated in [6]. In [7], the authors proposed a design of a fault-tolerant inverter by incorporating a fourth leg to replace the faulty leg. However, the use of additional power modules will inevitably increase the overall cost of the wind turbine. PMSG-based wind turbines use fully rated, back-to-

back converters to control the generated power. Therefore, conventional solutions used to improve the turbine on-time are not applicable with this topology. The bypass of power converters is not feasible since the PMSG cannot be connected to the grid without synchronization. Similarly, phase redundancy or converter redundancy will significantly increase the complexity of the design and the total cost of the wind turbine since it uses fully rated converters (FRCs). In this context, this paper proposes a new solution to ensure continuity of service for FRC wind turbines based on parallel interleaved converters (PICs) (Figure 1). This topology is based on the parallelization of standard three-phase inverters using coupled inductors [8]. These elements exhibit a high impedance with regard to differential-mode currents. They ensure a natural balancing of output currents between the two converters [9]. The proposed design can offer continuity of service through a fault-tolerant control strategy. In the event of a fault, the faulty converter is shut down and the wind turbine can continue operation at reduced power using only one of the two parallelized converters. Besides, each two-level converter is sized for half of the rated power of the wind turbine. Thus, compared to the solution based on redundant converters, the structure ensures continuity of service without a considerable increase in the cost of the electrical system. Section 2 presents the model of the PMSG-based wind turbine equipped with a parallel interleaved converter. Section 3 gives the conventional control strategy of the generator-side converter based on PI regulation. An LQ controller is synthesized to control the grid current components. In Section 4, the fault detection method is presented and the control strategy during faults is developed. Finally, the transient performances of the wind turbine are evaluated during power switch faults.

2. Model of the wind energy conversion system

Figure 1 shows the proposed configuration of the direct drive wind turbine, in which the generator-side converter is made with the parallel interleaved topology. DC links of the two interleaved converters are separated and each of them supplies a two-level converter. Grid-side converters (GrSC) are connected to the grid through two LCL filters and a three-windings transformer. Power limitation is achieved by a pitch servomechanism, which controls the rotor blade angle β. A torque controller is used to achieve variable speed operation of the PMSG. Using measurement of wind speed U and the rotor rotational speed Ω, an MPPT algorithm is used to calculate the torque reference T_{em}^{*}. Linear quadratic regulation is used to control the currents injected to the grid by the two grid-side converters. For each back-to-back converter, two relays are inserted in series with output phases. If a power switch fault is detected, the fault detection block inhibits the operation of the digital PWM blocks controlling the faulty back-to-back converters through signals $flt1$ and $flt2$. Then control signals RG_i are used to switch off the relays and isolate the defective conversion path. Next, through signal sw, a power set-point relative to the pitch angle controller is limited to half of the rated power ($P_r/2$). Similarly, an electromagnetic torque reference is limited to half of the rated value. Control signals RG_i, $flti$, and sw are generated by the control reconfiguration block, which will be detailed in Section 4. In the following, a brief description of the wind system components is given and the different control blocks are detailed.

2.1. Three-blade rotor

Using actuator disc theory, the aerodynamic torque developed by the rotor is given by [10]:

$$T_{mec} = \frac{1}{2}\rho\pi R^3 U^2 \frac{C_p(\lambda,\beta)}{\lambda}. \tag{1}$$

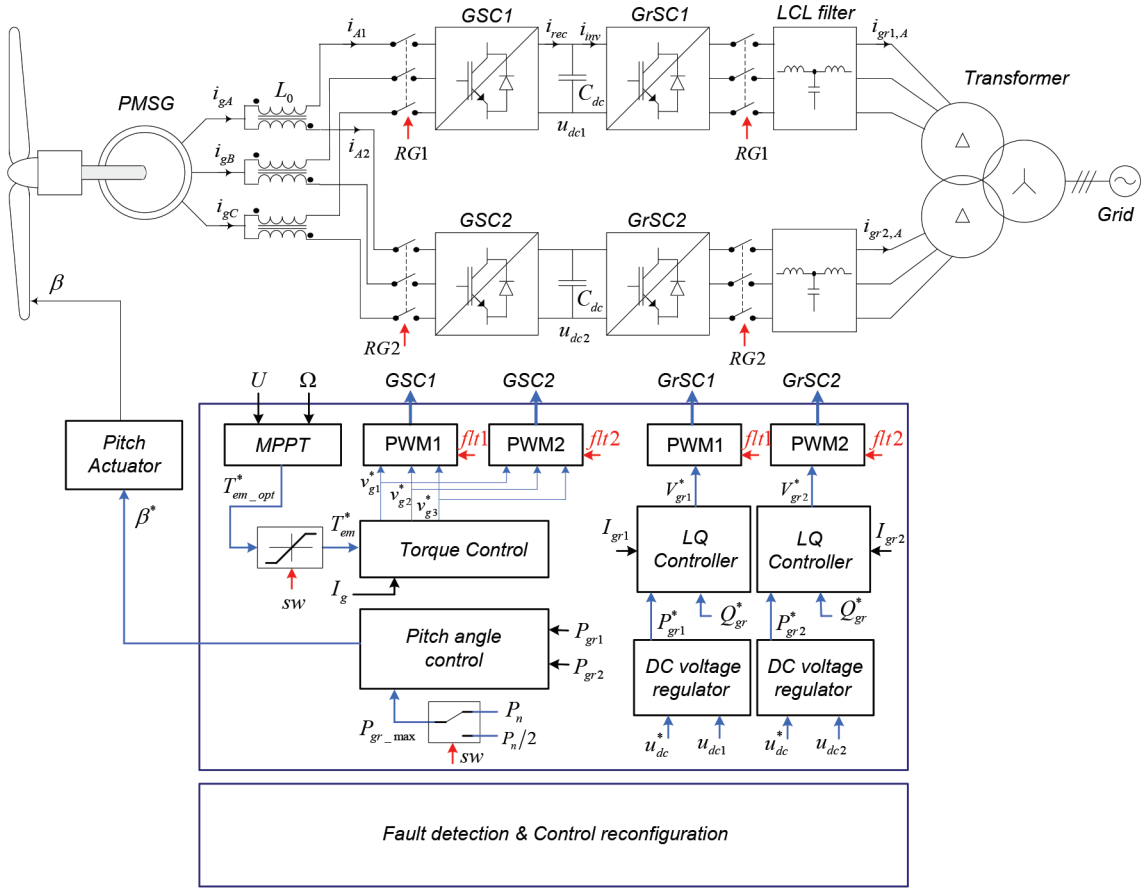

Figure 1. Topology of the 2 MW direct drive wind turbine and block diagram of the control strategy.

In Eq. (1), U, ρ, and R stand for, respectively, the wind speed, the air density, and the radius of the rotor. C_p is the power coefficient, which depends on the blade pitch angle and the tip speed ratio λ. λ is calculated by the following relation, in which Ω stands for the rotational speed of the three-blade rotor:

$$\lambda = \frac{\Omega R}{U}, \tag{2}$$

In [10], the authors proposed an analytical expression to represent the aerodynamic behavior of the rotor. According to this model, power coefficient C_p is approximated by the following relation:

$$C_p(\lambda, \beta) = c_1 \left(\frac{c_2}{\gamma_i} - c_3\beta - c_4\beta^{c_5} - c_6 \right) e^{-\frac{c_7}{\gamma_i}}, \tag{3}$$

with $\frac{1}{\gamma_i} = \frac{1}{\lambda + c_8\beta} + \frac{c_9}{\beta^3+1}$. Parameters c_i of Eq. (10) are taken from [10].

2.2. Pitch angle actuator

The pitch mechanism is used to turn the angle of attack of the blades with respect to the wind speed direction. Thus, the power recovered from the kinetic energy of the wind can be limited to the rated power of the generator. This mechanism should act rapidly whenever the wind speed exceeds the rated value. Typically, the maximum

variation rate of the pitch angle β is $\pm 10^{\circ}/s$ [10]. In this paper, a first-order system is used to model the pitch actuator dynamics (Figure 2).

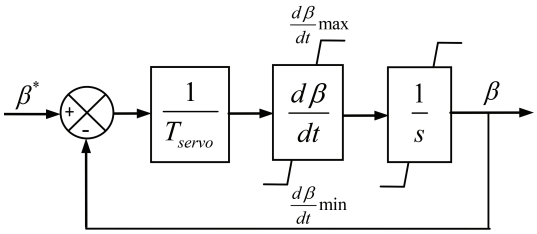

Figure 2. Model of the pitch actuator.

2.3. Permanent magnet synchronous generator

The multipolar PMSG is modeled in the dq rotative frame. The d-axis is aligned with the rotor flux. Using power invariant transformation, voltage equations of the stator are expressed by [11]:

$$v_{gd} = -R_g i_{gd} + \dot{\psi}_{gd} - \psi_{gq} p\Omega, \tag{4}$$

$$v_{gq} = -R_g i_{gq} + \dot{\psi}_{gq} + \psi_{gd} p\Omega. \tag{5}$$

R_g represents the resistance of stator windings and p the number of pole pairs. The flux components of the stator are given by:

$$\psi_{gd} = -L_d i_{gd} + \hat{\psi}_v, \tag{6}$$

$$\psi_{gq} = -L_q i_{gq}. \tag{7}$$

The rotor dynamics and the electromagnetic torque created by the generator are given by the following relations:

$$J_{tot}\frac{d\Omega}{dt} + f\Omega = T_{mec} - T_{em}, \tag{8}$$

$$T_{em} = p\left(\hat{\psi}_v i_{gq} + (L_q - L_d) i_{gq} i_{gd}\right), \tag{9}$$

where J_{tot} is the total inertia of the rotor and f is the friction coefficient.

2.4. Parallel interleaved converter

The generator-side converter ensures the control of the electromagnetic torque to achieve variable speed operation. Grid-side converters are used to control active and reactive powers injected to the grid. The parallel interleaved topology allows the design of more powerful wind turbines, because phase currents are equally shared between the parallelized two-level converters [12]. Besides, carrier signals of both VSCs are phase-shifted by 180°, significantly reducing the harmonic content of the output voltage, as in [13] and [14]. However, carrier interleaving causes high voltage spikes between output voltages v_{A1} and v_{A2} of the two converters (Figure 1). This would result in high differential mode currents circulating between the two VSCs. Differential mode

currents are limited using coupled magnetic elements as shown in Figure 1. The magnetic coupling between the two inductors can be represented by the equivalent circuit of Figure 3, in which copper losses are neglected.

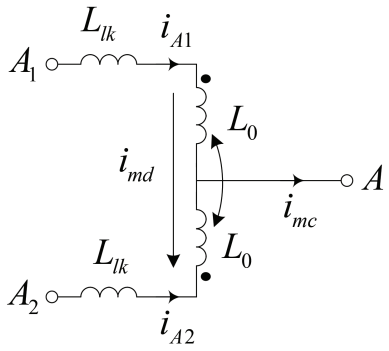

Figure 3. Equivalent circuit of two coupled inductors.

i_{A1} and i_{A2} stand for output currents of phases $A1$ and $A2$ of the two inverters. The output currents can be expressed as functions of differential-mode current i_{md} and common-modei_{mc} current:

$$i_{A1} = \frac{i_{mc}}{2} + i_{md}, \tag{10}$$

$$i_{A2} = \frac{i_{mc}}{2} - i_{md}. \tag{11}$$

The two coils are assumed to share the same number of turns. Consequently, relations between the self-inductance L_s, the mutual inductance L_0, and the leakage inductance L_{lk} are given by:

$$L_0 = kL_s, \tag{12}$$

$$L_{lk} = (1-k)\, L_s, \tag{13}$$

where k is the mutual coupling coefficient, which is close to 1. The two coils are wound on a magnetic core so that the flux created by common-mode currents is canceled out [15]. The voltage across the two terminals $A1$ and $A2$ is given by:

$$v_{A1} - v_{A2} = r_0 \cdot i_{md} + (2L_{lk} + 4L_0)\, \frac{d}{dt} i_{md}. \tag{14}$$

The above relation relates the high impedance produced with regards to differential-mode current. This impedance is approximately equal to four times the mutual inductance L_0 multiplied by the pulsation. Voltage variations across the capacitors of the DC links are modeled using the following equation:

$$\frac{du_{dc1,2}}{dt} = \frac{1}{C_{dc}} \left(i_{rec1,2} - i_{inv1,2}\right). \tag{15}$$

2.5. LCL filter dynamics

In the rotating frame dq, synchronized with the angle θ_{gr} of the grid voltage, the differential equations describing the LCL filter dynamics are expressed using the state space representation from [16] and [17]:

$$\begin{bmatrix} \dot{x} = Ax + B_1 v + B_2 v_{gr} \\ y = Cx \end{bmatrix}. \tag{16}$$

In Eq. (16), $y = \begin{bmatrix} i_{grd} & i_{grq} \end{bmatrix}^T$ represents the grid current components, $v = \begin{bmatrix} v_{id} & v_{iq} \end{bmatrix}^T$ represents the voltage vector generated by the GrSC, and the vector $v_{gr} = \begin{bmatrix} v_{grd} & v_{grq} \end{bmatrix}^T$ expresses the grid voltages referred to the primary of the transformer. The matrix expressions of this system are written as:

$$A = \begin{pmatrix} 0 & \omega_{gr} & -1/L_1 & 0 & 0 & 0 \\ -\omega_{gr} & 0 & 0 & -1/L_1 & 0 & 0 \\ 1/C & 0 & 0 & \omega_{gr} & -1/C & 0 \\ 0 & 1/C & -\omega_{gr} & 0 & 0 & -1/C \\ 0 & 0 & 1/L_2 & 0 & -R_{gr}/L_2 & \omega_{gr} \\ 0 & 0 & 0 & 1/L_2 & \omega_{gr} & -R_{gr}/L_2 \end{pmatrix}, \; B_1 = \begin{pmatrix} 1/L_1 & 0 \\ 0 & 1/L_1 \\ 0 & 0 \\ 0 & 0 \\ 0 & 0 \\ 0 & 0 \end{pmatrix},$$

$$B_2 = \begin{pmatrix} 0 & 0 \\ 0 & 0 \\ 0 & 0 \\ 0 & 0 \\ -1/L_2 & 0 \\ 0 & -1/L_2 \end{pmatrix}, \; C = \begin{pmatrix} 0 & 0 \\ 0 & 0 \\ 0 & 0 \\ 0 & 0 \\ 1 & 0 \\ 0 & 1 \end{pmatrix}^T,$$

where L_1, L_2, and C are the inductive and the capacitive elements of the filter and ω_{gr} is the angular frequency of the grid voltage.

3. Control strategy of the wind turbine

3.1. Control strategy of the GSC

To maximize the power extracted from the wind, the rotational speed Ω of the wind turbine should be adjusted as a function of wind speed variations. This task is achieved by an MPPT algorithm, which delivers the electromagnetic torque reference T^*_{em}. This torque is controlled through the broadly used vector oriented control (VOC).

Figure 4 shows the structure of the conventional torque controller from [18] and [19]. By neglecting the reluctant term in the electromagnetic torque expression of Eq. (9), the q-axis current reference i^*_{gq} is calculated from the torque reference T^*_{em} using Eq. (17). The d-axis current reference i^*_{gd} is forced to zero:

$$i^*_{gq} = \frac{1}{p\hat{\psi}_v} T^*_{em}. \tag{17}$$

3.2. Pitch angle controller

Figure 5 shows the control loop of the pitch mechanism used to limit the output power of the wind turbine. In this work, the chosen control variable is the total active power injected to the grid P_{gr} [20]. This power represents the sum of output powers delivered by the two GrSCs, P_{gr1} and P_{gr2}. The reference angle $\beta*$ is generated from the difference between the maximal allowed power $P_{gr\_\max}$ and the grid power P_{gr} using a PI

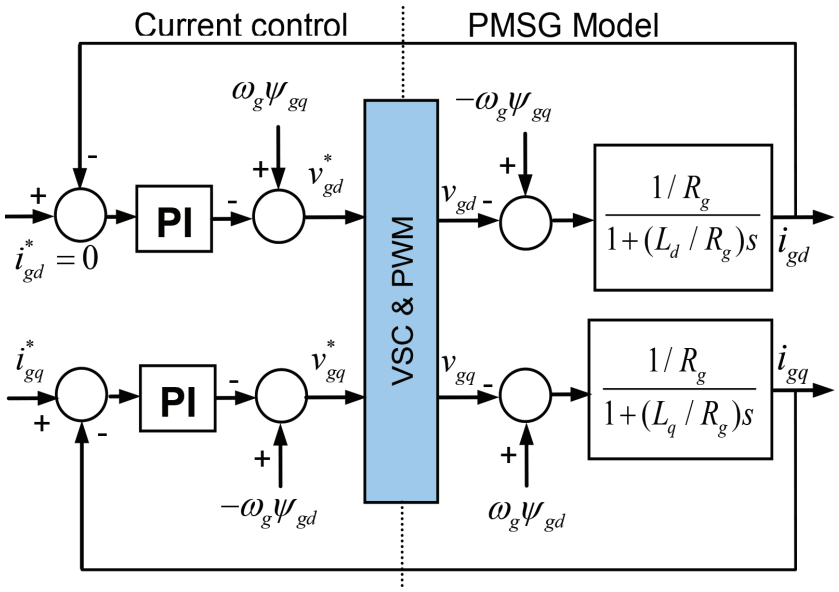

Figure 4. Conventional decoupled control of stator current.

regulator. When the wind turbine production is below the fixed setpoint $P_{gr\_\max}$, the pitch actuator turns the blade angle to reach the minimal limit $\beta_{\min}$ and the wind turbine operates with the maximal value of the power coefficient C_p. In this case, an anti-windup loop is used to prevent the saturation of the integral term. The use of a PI controller for the control of the blade-pitch angle has been extensively reported in the literature [20].

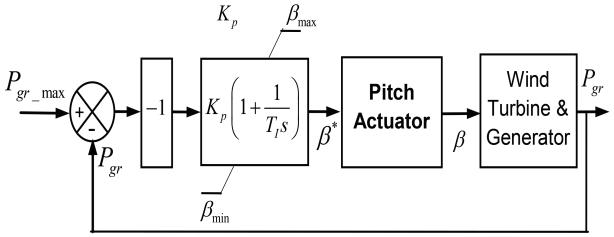

Figure 5. Control of the blade-pitch angle with anti-windup system.

3.3. Control strategy of the grid-side converters

The diagram of the LQ controller of grid currents is depicted in Figure 6. Current and voltage transducers are used to measure currents and voltages at the primary windings of the coupling transformer. The grid phase angle θ_{gr} is estimated through a phase locked loop (PLL). The lock is achieved by setting the direct grid voltage component v^*_{grd} to zero. A PI controller is used to correct the grid angle according to the error between v^*_{grd} and v_{grd}. Hence, the grid voltage vector is aligned with the q-axis of the rotating frame. This method has been already described in many works such as [21] and [22]. In Figure 6, L_d stands for the observer gain matrix and K_d represents the controller gain matrix. Φ and Γ are respectively the state matrix and the input matrix expressed in the discrete-time domain. Grid voltages $v_{gr} = \begin{bmatrix} v_{grd} & v_{grq} \end{bmatrix}^T$ are considered as a disturbance since their values cannot be controlled. The procedure to select the gain matrix has been discussed in many

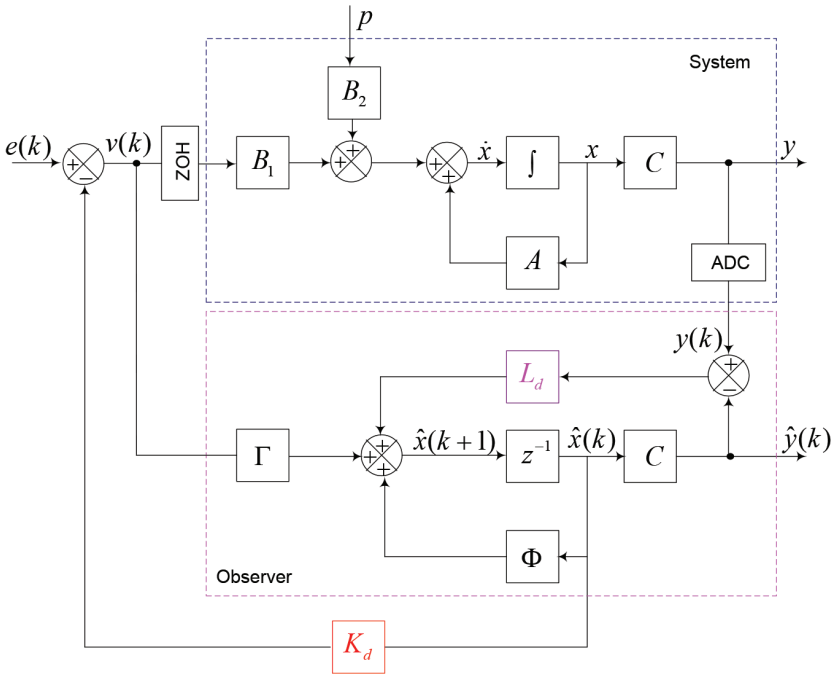

Figure 6. LQ control strategy of grid currents.

research works. In this paper, their values is set through the minimization of the cost functional given by:

$$J_{LQ} = \sum_{k=0}^{+\infty} \left(x_k^T Q x_k + u_k^T R u_k \right). \tag{18}$$

R is the control weighting matrix, which is positive-definite. Q is a semidefinite positive and it sets the transient response of state variables. Details for this method can be found in [21] and [22].

3.4. Control of DC bus voltages

Furthermore, voltages across the DC bus capacitors are controlled through an external control loop. Based on Eq. (15), variations of DC bus voltages are expressed by the following equation:

$$\frac{1}{2} C_{dc} \frac{du_{dc1,2}^2}{dt} = P_{rec1,2} - P_{gr1,2}. \tag{19}$$

In Eq. (19), the LCL filter dynamics are neglected and the active powers $P_{inv1,2}$ delivered by the GrSC are assumed equal to the active power $P_{gr1,2}^*$ delivered to the grid. Thus, considering that $u_{dc1,2}^2$ is the state variable to be controlled, with $P_{gr1,2}^*$ as the control input and $P_{rec1,2}$ as a disturbance, the control system of DC bus voltages is represented by the block diagram of Figure 7. τ_{CL} is the response time of grid current controllers.

4. Fault-tolerant control of the direct drive wind turbine

In this section, a fault detection method is proposed and the fault-tolerant design is developed. Mainly, power converter failure can take two forms: open-circuit failure and short-circuit failure. This paper is focused on

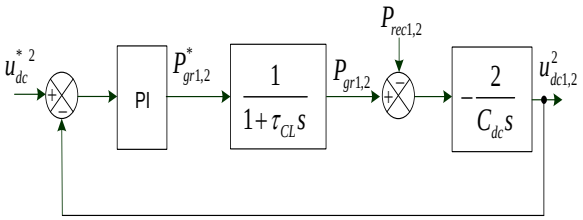

Figure 7. Control loop of DC bus voltages.

these two failure types to design the fault-tolerant control [23].

Many fault detection schemes for power converters were reported in the literature. In [24], the authors proposed a fault detection method for open-circuit faults as shown in Figure 8. Using the switching signals $T_{k,i}$ generated by the PWM blocks, voltages $v_{k_iO_i}$ $(k \in \{A, B, C\})$ between output terminals and the middle point of the DC link are estimated (see Figure 1). Estimated voltage for each converter leg is given by:

$$v_{k_iO_i,es} = (2T_{k,i} - 1)\frac{u_{dc}}{2}. \tag{20}$$

A comparator is used to calculate the difference between measured and estimated voltages. If the absolute value of the error signal exceeds a certain threshold h for a long enough time period N, then it is assumed that the converter has undergone a switching device failure. The threshold h and the observation time N are introduced to prevent false fault detection. Indeed, there is always an inevitable difference between real and estimated voltages caused by the falling and rising times of switches, dead times, and overvoltages due to stray inductances. This scheme can also be used to identify short-circuit faults if fast-acting fuses are inserted in series with each switching device [24].

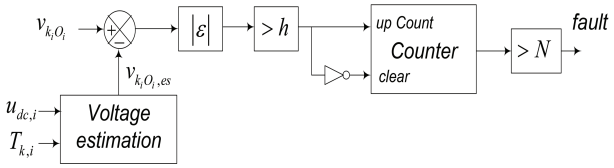

Figure 8. Fault detection scheme for two-level converters as presented in [24].

However, for the proposed wind system, the detection scheme of Figure 8 will excessively increase the complexity of the design since it includes 4 two-level converters, which means 12 legs overall. This leads to a large number of voltage transducers. Therefore, in this paper, a modified detection method is proposed in order to simplify the task of fault detection. Only DC bus voltages are required to detect switching faults in power converters, which are stacked in the back-to-back configuration. In the event of a fault occurring in any of the switching devices, DC bus voltages will be directly affected, being subject to oscillations or overvoltages. Thus, absolute values of the difference between measured DC bus voltages u_{dci} and the reference value u_{dc}^{*} are calculated as shown in Figure 9.

If any of the error signals exceeds a preselected threshold h, it is concluded that a switching device failure has occurred in one of the VSCs connected to the DC link enduring voltage oscillations. Hence, the control strategy of the wind turbine is reconfigured with the objective of isolating the faulty conversion path. An RS flip-flop is used to inhibit the PWM signals of the back-to-back converters in which the fault has been

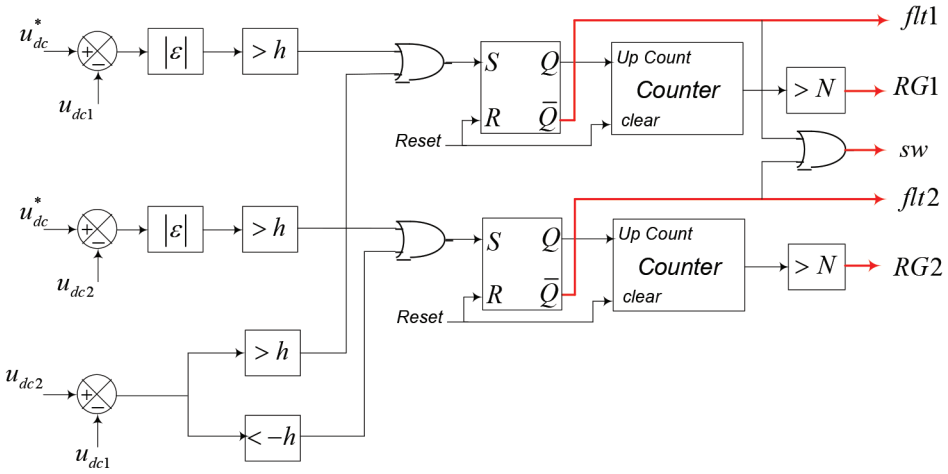

Figure 9. Fault detection and control reconfiguration for the direct drive wind turbine.

detected, for example using $flt1$ (see Figure 1). The same signal sw activates a selector, which reduces by half the maximal torque reference T^*_{em}. The signal sw limits the maximal power generated by the wind turbine to half of the rated power P_r. After a time delay N, the faulty back-to-back converter is disconnected from the wind system through control signal $RG1$. It is worth mentioning that the observation time N is introduced to prevent overvoltages created by transient currents that flow in the LCL filter elements. During the observation time, transitory currents will decay to zero since they are damped by discharging resistors, inserted in parallel with the capacitive elements of the filter. The same process takes place if an open-circuit fault occurs in the second conversion path. The performances of this fault-tolerant control are analyzed in the following section. The wind turbine operation is simulated during an open-circuit fault occurring in the GSC and in the GrSC. Then the scenario of a short-circuit failure is analyzed.

5. Results and performances

In this section, the operation of the wind system is analyzed. Two switch faults are simulated to evaluate the performances of the fault-tolerant control strategy. The model of the wind system and the global control algorithm are implemented in the MATLAB Platform 2013a. Simulation parameters are listed in the Table.

5.1. Open-circuit fault in the generator-side converter

Figure 10 shows the wind turbine behavior in the event of an open switch fault that occurs at the time of 0.04 s in generator-side converter GSC1. Through the signal sw, the electromagnetic torque is limited to half of the rated value as depicted in Figure 10a. As shown in Figure 10b, the difference between the two DC bus voltages, u_{dc1} and u_{dc2}, increases until it exceeds the threshold h. Thus, the fault is detected and the PWM signals of converters GSC1 and GrSC1 are inhibited through signal $flt1$. As a result of these control actions, the active power P_1 generated by grid-side converter GrSC1 gradually decreases to zero (Figure 10c). The total power delivered by the wind turbine is reduced to half of the rated value (Figure 10d). As can be seen from Figure 10e and Figure 10f, power transfer from the defective to the safe back-to-back converter does not induce overcurrents for both converters connected to the grid. After an observation time N of 30 ms, $RG1$ is switched off and the defective back-to-back converter is totally isolated from the electrical subsystem. The observation

Table 1. System numeric parameters.

Parameter	Symbol	Value	Unit	Parameter	Symbol	Value	Unit
Wind Turbine				Longitudinal reactance	X_d	1.49	p.u.
Base power	P_B	2.2	MW	Transversal reactance	X_q	0.93	p.u
Rotor radius	R	36	m	**Electrical elements**			
Rated rotational speed	Ω_r	2.52	rd.s^{-1}	Base voltage	V_{BC}	400	V
Rated wind speed	U_r	12.5	m/s	Base frequency	f	50	Hz
PMSG				Mutual reactance of coupled inductors	X_0	0.65	p.u.
Base power	S_B	2.02	MVA	Leakage reactance of coupled inductors	X_{lk}	0.03	p.u.
Base voltage	V_B	1000	V	Filter inductive reactance	X_{L1},X_{L2}	0.26	p.u.
Pole pairs	p	32	-	Filter capacitive reactance	X_C	380	p.u.
Nominal frequency	f_g	13	Hz	DC base voltage	U_{DC_b}	1127	V
Rotor flux	ψ_v	1.5	p.u.	DC bus capacitors	X_{DC}	0.74	p.u.
Stator resistance	R_g	0.02	p.u.				

time is chosen higher than the dynamics of the LCL filter to avoid overvoltages during the relay switching. The wind turbine continues to produce energy through the second back-to-back converter (Figure 10g). Hence, the proposed fault-tolerant control ensures the continuity of service and the equipment safety.

5.2. Open-circuit fault in grid-side converter GrSC1

Figure 11 shows the wind turbine behavior in the event of an open switch fault that arises in grid-side converter GrSC1. This failure leads to unbalanced currents in the LCL filter elements. Unbalanced currents provoke overvoltage across the DC link connected to the defective converter. Hence, the fault is detected and PWM signals of converters GSC1 and GrSC1 are inhibited through signal $flt1$. Simultaneously, through signal sw, the maximum electromagnetic torque is reduced to 0.5 p.u. (Figure 11a). Currents produced by GrSC1 decay gradually to zero and the voltage u_{dc2} returns to its initial level under the effect of the control loop (Figure 11b). After a certain period of time, the system becomes stable and the power injected to the grid is totally fed by the second back-to-back converter (Figure 11c). The total produced power is reduced to half of the rated value (Figure 11d). The peak value of converter currents is slightly higher than the rated value during the transient state as shown in Figure 11e and Figure 11f. The switching off of relays $RG1$ does not affect the wind turbine operation and it isolates the defective back-to-back converter. After fault clearance, the wind turbine delivers sinusoidal currents to the grid as shown in Figure 11g. Hence, it can be concluded that the proposed fault-tolerant control gives satisfactory results in terms of availability improvement.

5.3. Short-circuit fault in the generator-side converter

Figure 12 shows the wind turbine response during a short-circuit failure in GSC1. Figure 12a shows the variations of the stator currents of the PMSG. As can be observed in Figure 12b, the short circuit causes a rapid discharge

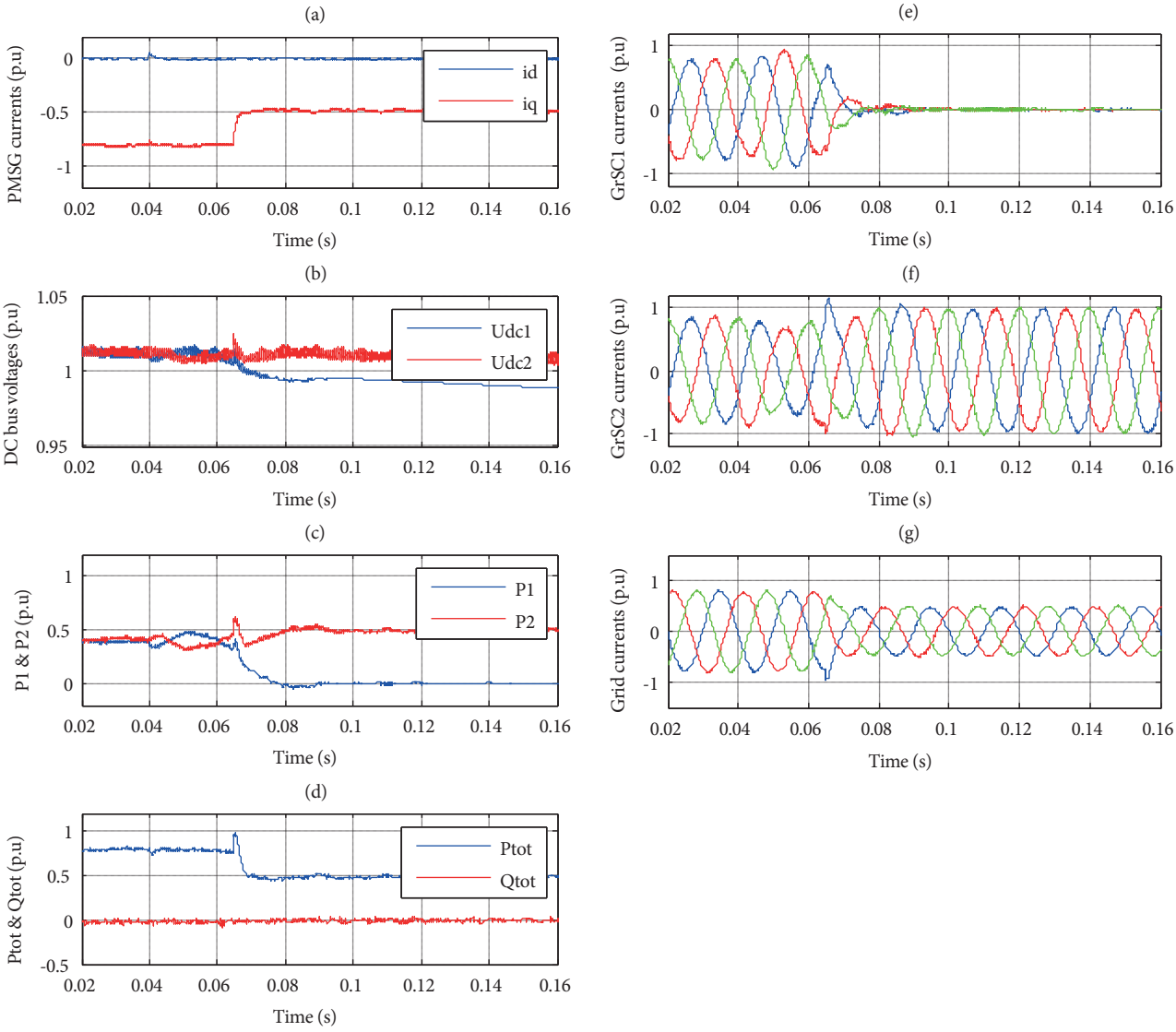

Figure 10. Operation of the wind turbine during an open switch fault in the generator-side converter GSC1. (a) components of stator currents. (b) DC bus voltages. (c) Active powers delivered by the grid-side converters. (d) Active and reactive powers injected to the grid. (e) Grid currents delivered by GrSC1. (f) Grid currents delivered by GrSC2. (g) Grid currents at the secondary windings of the transformer.

of DC link capacitor C_{dc1}. Thus, the fault is detected and the control signal $flt1$ inhibits the PWM output signals of GSC1 and GrSC1. The short circuit results in power oscillations in the two grid-side converters (Figure 12c). This perturbation is transmitted to active and reactive power delivered to the grid (Figure 12d). Figure 12e and Figure 12f show currents in GrSC1 and GrSC2, which undergo transient oscillations. However, after the transient period, the wind system returns back to stable operation as shown in Figure 12g. Hence, it is concluded that the wind system can overcome this fault type with the proposed fault-tolerant control strategy.

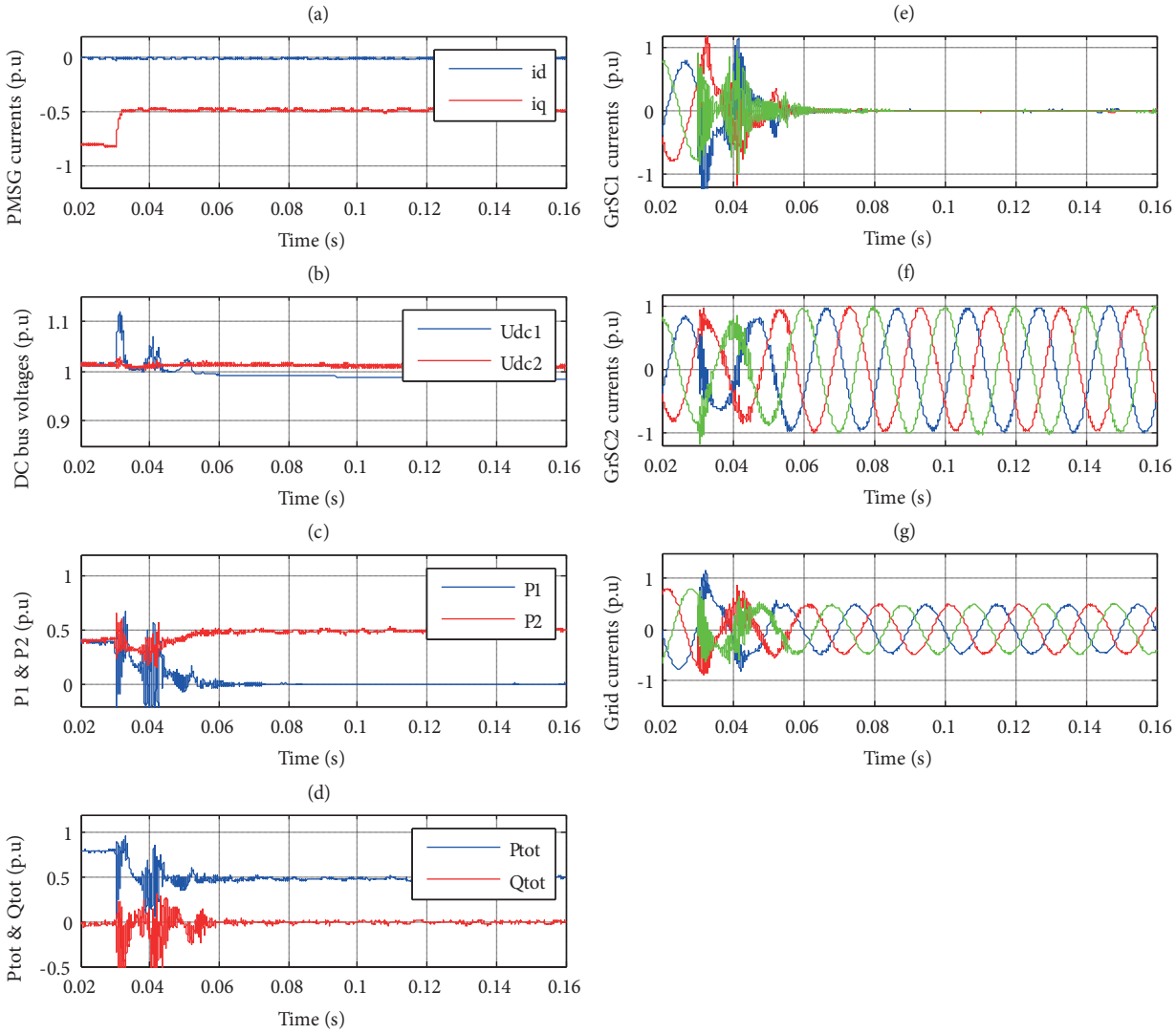

Figure 11. Operation of the wind turbine during an open switch fault in grid-side converter GrSC1. (a) Components of stator currents. (b) DC bus voltages. (c) Active powers delivered by the grid-side converters. (d) Active and reactive powers injected to the grid. (e) Grid currents delivered by GrSC1. (f) Grid currents delivered by GrSC2. (g) Grid currents at the secondary windings of the transformer.

6. Conclusion

This paper proposes a new configuration for direct-drive wind turbines based on parallel interleaved converters with separate DC links. The aim of this structure is to improve the availability of such wind systems. The implementation of this topology does not raise any technological challenges since it is based on the well-established technology of two-level converters. The used converters are sized for half of the rated power of the wind turbine. Thus, the cost of additional power modules is compensated by their reduced current ratings. Furthermore, the proposed configuration improves the availability of direct-drive wind turbines. It offers continuity of service in the event of a switching device failure. Indeed, through the fault-tolerant control strategy, control signals RG_i and $flti$ isolate the defective conversion path. The wind turbine can continue to deliver power to the grid with a maximal value equal to half of the rated power ($P_r/2$). The control methods of

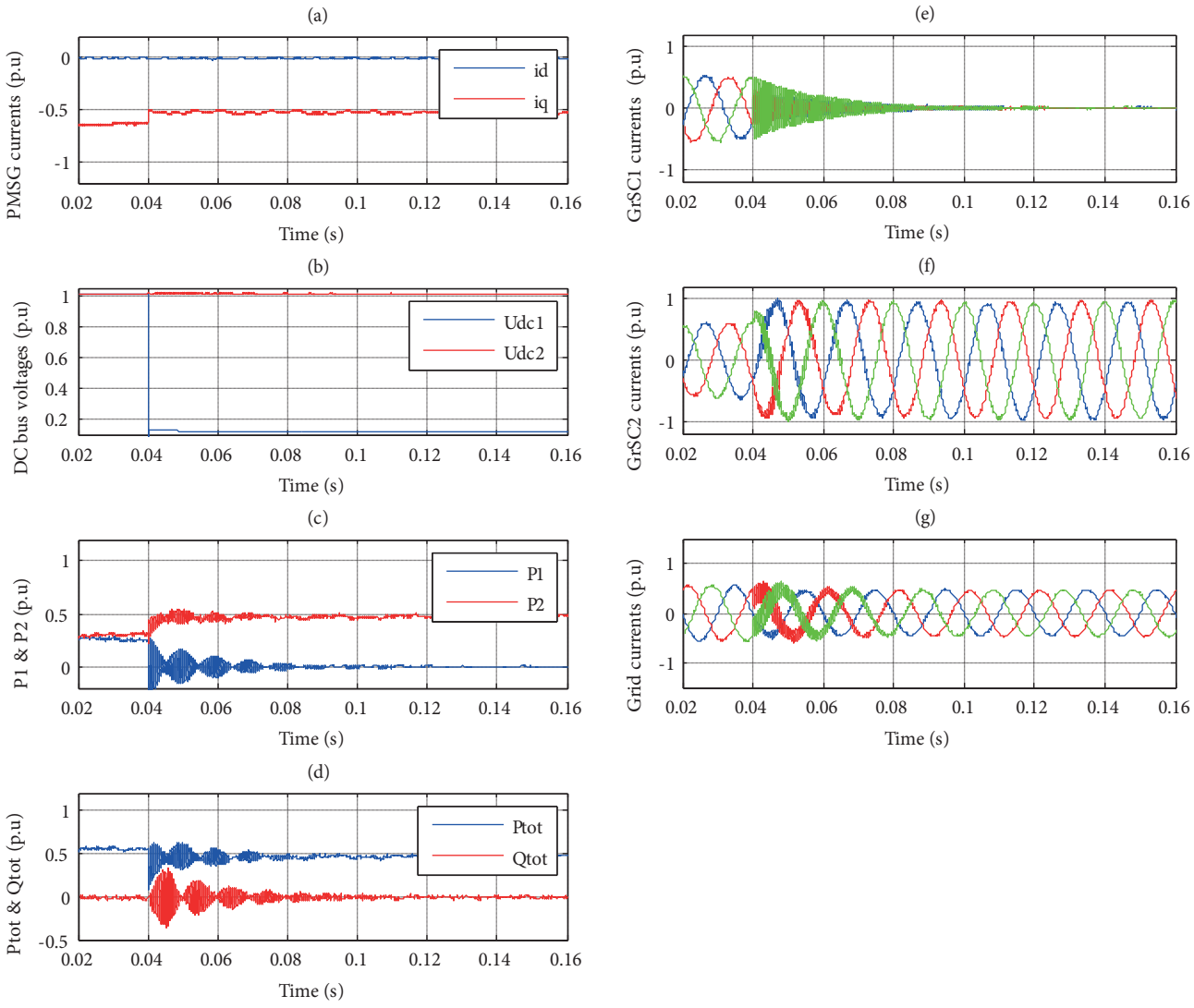

Figure 12. Operation of the wind turbine during a short-circuit failure in generator-side converter GSC1. (a) Components of stator currents. (b) DC bus voltages. (c) Active powers delivered by the grid-side converters. (d) Active and reactive powers injected to the grid. (e) Grid currents delivered by GrSC1. (f) Grid currents delivered by GrSC2. (g) Grid currents at the secondary windings of the transformer.

the generator and the grid-side converters were presented in this paper. Common LQ control was used to achieve effective control of grid currents. The performances of the fault-tolerant control were evaluated by simulating an open switch fault and a short-circuit failure of power switches. In both cases, the control reconfiguration technique gives satisfactory results since it ensures the continuity of generation and the magnitude of transient currents remains limited. In addition, it allows the isolation of the defective part of the electrical subsystem.

References

[1] Fischer K, Besnard F, Bertling L. Reliability-centered maintenance for wind turbines based on statistical analysis and practical experience. IEEE Transactions on Energy Conversion 2012; 27: 184-195.

[2] Pfaffel S, Faulstich S, Rohrig K. Performance and reliability of wind turbines: a review. Energies 2017; 10: 1-27.

[3] Pelka K, Fischer K. Failure behaviour of power converters in wind turbines. In: German Wind Energy Conference; Bremen, Germany; 2017. pp. 1-5.

[4] Odgaard PF, Stoustrup J, Kinnaert M. Fault-tolerant control of wind turbines: a benchmark model. IEEE Transactions on Control Systems Technology 2013; 21: 1168–1181.

[5] El-Shimy M. Wind Energy Conversion Systems: Reliability Perspective. Encyclopedia of Energy Engineering and Technology. New York, NY, USA: CRC Press, 2015.

[6] El-Shimy M. Alternative configurations for induction-generator based geared wind turbine systems for reliability and availability improvement. In: Proceedings of the 14th International Middle East Power Systems Conference; Cairo, Egypt; 2010. pp. 538-543.

[7] Moujahed M, Ben Azza H, Frifita K, Jemli M, Boussak M. Fault detection and fault-tolerant control of power converter fed PMSM. Electrical Engineering 2016; 98: 121-131.

[8] Okedu K. Enhancing DFIG wind turbine during three-phase fault using parallel interleaved converters and dynamic resistor. IET Renewable Power Generation 2016; 10: 1211–1219.

[9] Quan Z, Li Yun W. Suppressing zero-sequence circulating current of modular interleaved three-phase converters using carrier phase shift PWM. IEEE Transactions on Industry Applications 2017; 53: 3782-3792.

[10] Knudsen H, Nielsen N, Ackermann T. Wind Power in Power Systems. Chichester, UK: John Wiley, 2005.

[11] Boldea I. Synchronous Generators. New York, NY, USA: CRC Press, 2006.

[12] Ewanchuk J, Salmon J. Three-limb coupled inductor operation for paralleled multi-level three-phase voltage sourced inverters. IEEE Transactions on Industrial Electronics 2013; 60: 1979–1988.

[13] Lakhsmi S, Raja SR. Observer-based controller for current mode control of an interleaved boost converter. Turkish Journal of Electrical Engineering and Computer Sciences 2014; 8: 341–352.

[14] Gohil G, Bede L, Teodorescu R, Kerekes T, Blaabjerg F. Flux balancing scheme for PD modulated parallel interleaved inverters. IEEE Transactions on Power Electronics 2017; 32: 3442–3457.

[15] Laka A, Barrena JA, Zabalza JC, Vidal R, Izurza-Moreno P. Isolated double-twin VSC topology using three-phase IPTs for high-power applications. IEEE Transactions on Power Electronics 2014; 29: 5761-5769.

[16] Abbes M, Allagui M. Centralized control strategy for energy maximization of large array wind turbines. Sustainable Cities and Society 2016; 25: 82-89.

[17] Huerta F, Pérez J, Cóbreces S, Rizo M. Frequency-adaptive multiresonant LQG state-feedback current controller for LCL-filtered VSCs under distorted grid voltages. IEEE Transactions on Industrial Electronics 2018; 65: 8433-8444.

[18] Qiao W, Yang X, Gong X. Wind speed and rotor position sensorless control for direct-drive PMG wind turbines. IEEE Transactions on Industry Applications 2012; 48: 3-11.

[19] Yang J, Song D, Han H, Tong P, Zhou L. Integrated control of fuzzy logic and model-based approach for variable-speed wind turbine. Turkish Journal of Electrical Engineering and Computer Sciences 2015; 23: 1715–1734.

[20] Abbes M, Allagui M, Hasnaoui O. An aggregate model of PMSG-based, grid connected wind farm: investigation of LVRT capabilities. In: Sixth International Renewable Energy Congress; Sousse, Tunisia; 2015.

[21] Levine WS. The Control Handbook. Boca Raton, FL, USA: CRC Press, 2005.

[22] Huerta F, Pizarro D, Cobreces S, Rodriguez FJ, Girón C et al. LQG servo controller for the current control of LCL grid-connected voltage-source converters. IEEE Transactions on Industrial Electronics 2012; 59: 4272-4284.

[23] Busca C, Teodorescu R, Blaabjerg F, Munk-Nielsen S, Helle L et al. An overview of the reliability prediction related aspects of high power IGBTs in wind power applications. Microelectronics Reliability 2011; 51: 1903-1907.

[24] Wu R, Blaajberg F, Wang H, Liserre M. Catastrophic failure and fault-tolerant design of IGBT power electronic converters - An overview. In: 39th Annual Conference of the IEEE Industrial Electronics Society; Vienna, Austria; 2013. pp. 507-513.